The Cryosphere Discuss., 8, 5875–5910, 2014
www.the-cryosphere-discuss.net/8/5875/2014/
doi:10.5194/tcd-8-5875-2014

The Cryosphere Discussions
Open Access

Spatiotemporal variations in the surface velocities of Antarctic Peninsula glaciers

J. Chen[1,2], **C. Q. Ke**[1,2], **and Z. D. Shao**[1,2]

[1]Jiangsu Provincial Key Laboratory of Geographic Information Science and Technology, Nanjing University, Nanjing, 210023, China
[2]Key Laboratory for Satellite Mapping Technology and Applications of State Administration of Surveying, Mapping and Geoinformation of China, Nanjing University, Nanjing, 210023, China

Received: 25 October 2014 – Accepted: 2 November 2014 – Published: 25 November 2014

Correspondence to: C. Q. Ke (kecq@nju.edu.cn)

Published by Copernicus Publications on behalf of the European Geosciences Union.

Abstract

Velocity is an important parameter for the estimation of glacier mass balance, which directly signals the response of glaciers to climate change. Antarctic ice sheet movement and the associated spatiotemporal velocity variations are of great significance to global sea level rise. In this study, we estimate Antarctic Peninsula glacier velocities using the co-registration of optically sensed images and correlation (hereafter referred to as COSI-Corr) based on moderate-resolution imaging spectroradiometer Level 1B data (hereafter referred to as MODIS L1B). The results show that the glaciers of Graham Land and the Larsen Ice Shelf have substantially different velocity features. The Graham Land glaciers primarily flow from the peninsula ridge towards the Weddell Sea and Bellingshausen Sea on the east and west sides, respectively. There are very large velocity variations among the different ice streams, with a minimum of $< 20\,\mathrm{m\,a^{-1}}$ and a maximum of $1500\,\mathrm{m\,a^{-1}}$ (with an average of 100–$150\,\mathrm{m\,a^{-1}}$). Over the period 2000–2012, the glaciers of Graham Land accelerated in the south but slowed down in the north. In contrast, the Larsen Ice Shelf flows in a relatively uniform direction, mainly towards the northeast into the Weddell Sea. Its average velocity is 750–$800\,\mathrm{m\,a^{-1}}$ and the maximum is $> 1500\,\mathrm{m\,a^{-1}}$. During the period 2000–2012, the Larsen Ice Shelf experienced significant acceleration. The use of COSI-Corr based on MODIS L1B data is suitable for glacier velocity monitoring on the Antarctic Peninsula over long time series and large spatial scales. This method is clearly advantageous for analysing macroscale spatiotemporal variations in glacier movement.

1 Introduction

The Antarctic ice sheet is closely related to significant problems, such as global climate and eco-environment, as well as the future development of human society (Lucchitta et al., 1993). With the intensification of global warming, glaciers are playing an increasingly evident role as an amplifier and indicator of global climate change (Shi and Liu,

TCD
8, 5875–5910, 2014

2000). Glacial velocity is an important factor influencing ice flux (Rosenau et al., 2012) and an important parameter in the estimation of Antarctic ice sheet mass balance. Additionally, glacial velocity directly signals the response of the Antarctic ice sheet to global climate change. Thus, studies on the velocities of Antarctic glaciers have become important for developing global sea level rise models (Chen et al., 2007).

Methods for monitoring Antarctic ice velocities are mainly classified into two categories: in situ measurement and remote sensing monitoring. Stake measurement is the first method of in situ measurement used for monitoring Antarctic ice velocities (Hofmann et al., 1964; Dorrer et al., 1969). At present, global positioning system (hereafter referred to as GPS) technology has become the most important tool for field measurements of Antarctic glacier dynamics and ice surface terrain (Manson et al., 2000). However, the harsh environment, high cost of field observation, and a relatively short retest period have substantially limited in situ measurements (Urbini, 2008; Sunil, 2007). Remote sensing methods, including microwave and optical remote sensing, allow for rapid development of Antarctic ice velocity measurements using synthetic aperture radar (hereafter referred to as SAR) data (Kimura et al., 2004; Dong et al., 2004; Pattyn and Derauw, 2002). By means of interferometric SAR (hereafter referred to as InSAR) and feature tracking, researchers have obtained ice velocity measurements of the entire Antarctic ice sheet and generated an Antarctic ice sheet velocity profile (Rignot et al., 2011). SAR data are independent of weather conditions (clouds and rain) and have high accuracy (Ke et al., 2013). Nonetheless, the frequent melting behaviour of glaciers and snow on the Antarctic Peninsula is likely to cause a loss of coherence in SAR images, accounting for the longer observation period of SAR feature tracking method than the InSAR method. Additionally, the impact of incidence angle in steep terrains can limit the visibility of some glaciers in SAR images, and a high-resolution digital elevation model (hereafter referred to as DEM) is needed for terrain correction. Therefore, active microwave remote sensing is highly suitable for velocity monitoring over relatively short periods (Scheuchl et al., 2012).

TCD
8, 5875–5910, 2014

Co-registration of optically sensed images and correlation (COSI-Corr) is a methodology based on the calculation of grayscale pixel values using a simple algorithm. COSI-Corr is advantageous because of its larger number of optical remote sensors, longer time series, and rich data resources. It is therefore more suitable than SAR monitoring methods for estimating the speed of glacial movement and the analysis of relevant spatiotemporal variations over long time series (Ferrigno et al., 1998; Liu et al., 2012). Because the accuracy of COSI-Corr is primarily determined by the spatial resolution of a pixel, Antarctic ice sheet velocity monitoring based on optical images mostly adopts high-resolution images, such as TM/ETM (Ferrigno et al., 1994), ASTER (Tiwari et al., 2012), and SPOT (Ahn and Howat, 2010). Additionally, due to differences in the attitudes of satellites, system errors occur during image splicing, and coordination registration errors between different images affect the accuracy of COSI-Corr. Thus, study on cross-correlation algorithms becomes the focus for improving the accuracy of COSI-Corr. For example, Heid and Kaab (2012) compared and evaluated six different matching algorithms: normalized cross-correlation operated in the spatial domain (NCC), cross-correlation operated in the frequency domain using Fast Fourier Transform (CCF), phase correlation operated in the frequency domain using Fast Fourier Transform (PC), cross-correlation operated in the frequency domain using Fast Fourier Transform on orientation images (CCF-O), phase correlation operated in the frequency domain using Fast Fourier Transform on orientation images (PC-O) and the phase correlation algorithm used in COSI-Corr. The use of high-resolution images for monitoring the velocity of single ice streams on the Antarctic Peninsula has also resulted in important findings. For example, the study by Scambos et al. (2004) estimated the velocities of the Crane Glacier using TM images. As the collapse of the Antarctic ice shelf intensifies, great progress has been made in measuring ice shelf velocities (Yu et al., 2010; Scheuchl et al., 2012). However, few studies have been reported for the Antarctic ice sheet with regard to ice velocities on larger spatial scales over longer time spans.

Antarctic Peninsula glaciers are polar continental glaciers that have high surface velocities (Khazendar et al., 2011). For these glaciers, MODIS data of 250 m resolution

TCD
8, 5875–5910, 2014

meet the matching criteria of feature tracking. Additionally, medium-resolution images have the following advantages: (1) single images can cover a broader area, thereby reducing errors in cross-correlations caused by data splicing and coordination registration; and (2) the larger field of view allows for data coverage multiple times per day in the same area of the polar region, facilitating the selection of high-quality data from the period with minimum cloud (Haug et al., 2010). In the present study, we use COSI-Corr to estimate Antarctic Peninsula glacier surface velocities and analyse their spatiotemporal variations over the period 2000–2012 based on medium-resolution MODIS L1B data.

2 Study area

The Antarctic Peninsula in West Antarctica (Fig. 1) is the largest peninsula of the Antarctic continent, stretching the farthest northward into the sea (63° S). In this region, the strata belong to a Cenozoic fold belt, and the bedrock is undulatory. The average annual rainfall is up to 500–600 mm. The peninsula, also known as Maritime Antarctica, is the warmest place with the most snowfall on the Antarctic continent. Over the period 1952–2000, the Antarctic Peninsula experienced a temperature rise of 5.6 °C (Turner et al., 2005), and during 1955–1998, there was a sea surface temperature rise of more than 1 °C in the Pacific Ocean to the west of the peninsula (Meredith and King, 2005). Due to this temperature increase, the area lost from the Larsen Ice Shelf since 1986 has exceeded 8500 km^2 (Pritchard and Vaughan, 2007). The collapse of the Larsen Ice Shelf has caused substantial ice loss in upstream supplies of the Antarctic Peninsula, e.g. up to $6.8 \pm 0.3\,km^3\,a^{-1}$ in the Fleming Glacier, which accelerated by 50 % relative to the velocity in 1974 (Rignot et al., 2004). Pritchard and Vaughan (2007) monitored the velocities of more than 300 glaciers on the Antarctic Peninsula and found an average acceleration of 12 % between 1992 and 2005, mainly due to downstream glacier mass loss. These authors further estimated the mass output of the Antarctic Peninsula to be $60 \pm 46\,Gt\,a^{-1}$ in 2005 (Pritchard and Vaughan, 2007). If the marine ice sheet in West

TCD
8, 5875–5910, 2014

Antarctica completely disintegrates, sea level will rise 3.3 m (Bamber et al., 2009). In short, Antarctic Peninsula glacier surface velocities have great implications for estimating Antarctic ice sheet mass balance and the study of global climate change (Skvarca et al., 1999; Osmanoglu et al., 2013).

The Antarctic Peninsula has a number of affiliated islands that cover relatively small areas. In medium-resolution optical images, each of these affiliated islands occupies a very limited number of pixels, whereas the scope of the window set for cross-correlation calculation is large relative to the island pixels. Thus, the affiliated islands are neglected in this study to improve the accuracy of computation.

Due to factors such as temperature and ocean currents, the melt lines of ice shelves on the Antarctic Peninsula vary widely during different years (Fig. 2). If surface features of varying natures are used for feature tracking based on the digital number (hereafter referred to as DN) value of pixel, large errors will arise in the calculated results. Hence, we extract the minimum freeze/melt lines of sea ice during five different periods as the scope of cross-correlation calculation, mainly covering Graham Land and the Larsen Ice Shelf (10.5 km^2).

3 Data

The use of COSI-Corr requires: (1) at least two images in which the glacier surface texture can be observed and (2) precise geographic coordinates, with an image resolution superior to total glacier displacement during the observation period (Huang and Li, 2009). As long as the two conditions are satisfied, optical image cross-correlation can be calculated (Ferrigno et al., 1994; Erten et al., 2012). The continental glaciers on the Antarctic Peninsula have a significantly higher average velocity than mountain glaciers. Thus, medium-resolution MODIS data can meet the conditions for optical image feature tracking. In addition, MODIS data have advantages of free access, wide coverage, short revisit cycles, and long time series. These advantages can help choose suitable

TCD
8, 5875–5910, 2014

data for comparison studies over long time series, facilitating cross-correlation calculation in large areas of the Antarctic region.

The MODIS L1B data products are provided by US National Aeronautics and Space Administration (NASA). In accordance with the type of satellite carrier, the data can be divided into two categories: MOD02 (Terra-MODIS) and MYD02 (Aqua-MODIS). Here, we use band 1 data (spectral range: 620–670 nm) of the MOD02 product at 250 m resolution. Band 1 L1B data are products with geographic coordinates obtained after instrument calibration. However, "geographic data" and "scientific data" that record reflectivity are not connected, resulting in so-called bow-tie phenomena near the edge when displayed directly. It is thus necessary to connect the MOD02 and MOD03 data products (Geolocation 1 km) for geocoding prior to cross-correlation calculations. During calibration, the pixel values are synchronically converted from reflectance to DN values, ultimately producing images with precise geographic coordinates. Because the Antarctic Peninsula experiences cloudy, snowy weather and its winter months are strongly affected by the "polar night", it is difficult to obtain high-quality continuous images. Therefore, we choose images from 2000, 2003, 2006, 2009, and 2012 data associated with little or no clouds for glacier velocity estimation (Fig. 2, Table 1).

In addition, the Advanced Spaceborne Thermal Emission and Reflection Radiometer Global Digital Elevation Model (hereafter referred to as ASTER GDEM) within the study area is used, this version is developed in accordance with detailed Terra observations (Holger and Frank, 2012), almost 1.3 million scenes of ASTER VNIR data covering the Earth land surface between 83° N and 83° S latitudes acquired from 1999 to 2010 have been processed by stereo-correlating (Slater et al., 2009). The ASTER GDEM was released in geotiff format with geographic lat/long coordinates, the spatial resolution is 30 m and the vertical accuracy is 20 m (Kang and Feng, 2011), its latitude–longitude coordinate was referenced to UTM/WGS 84 and the elevations were computed with respect to the Earth Geopotential Model 1996 (EGM96) geoid (Ni et al., 2014), which meet the conditions for digital elevation calculations at larger spatial scales (ASTER GDEM data can be downloaded from the NASA web

TCD
8, 5875–5910, 2014

pages, http://asterweb.jpl.nasa.gov/gdem.asp or from the LPDAAC Global Data Explorer) (Djamel and Hammadi, 2014).

4 Methods

The estimation of ice velocity using COSI-Corr mainly involves four steps: in-plane displacement measurement, surface velocity calculation, three-dimensional (hereafter referred to as 3-D) terrain correction, and the displacement orientation conversion (Fig. 3).

4.1 Displacement measurement

Early images are used as the reference images, and late images serve as the search images. Grid segmentation is performed to divide the reference images into standard windows (cells). Windows (cells) of the same size that have the highest correlation are then identified from the search area of the search image. The displacement between the feature point of maximum correlation in the reference image and the matching point in the search image is determined after grid segmentation and the cross-correlation calculation. After completion of the cross-correlation calculation in one grid, it is shifted by a certain step size for continuous calculation in the next grid. This procedure eventually produces a raster data file with the step size as the pixel resolution and the matching feature points as the pixel values (Fig. 4). It should be noted that UTM projection (same length and width of each pixel) is adopted in the orthophoto coordinate system to facilitate grid segmentation. However, due to projection deformation in the polar regions, there is a necessity to convert the results of the cross-correlation calculations into polar azimuthal projection (different length and width of each pixel) prior to displacement and area measurements, which will ensure the accuracy of the measurement.

To improve the accuracy of correlation calculations, the grid size should be as large as possible and a larger number of pixels should be involved in the calculation. For

TCD
8, 5875–5910, 2014

example, the reference window for feature tracking of TM images in the Koxkar Baxi Glacier (average velocity $< 120\,\mathrm{m\,a^{-1}}$) is set to 32×32 pixels (Xu et al., 2011). Additionally, the search area should be enlarged as much as possible and the spatial scale of feature point matching can be extended to ensure that the possible maximum displacement of the glacier is included in the search area (Huang and Li, 2009). Haug et al. (2010) set the MODIS image-based search window to 44×44 pixels and the TM image-based search window to 350×350 pixels for the Larsen Ice Shelf. However, the Antarctic Peninsula glacier surfaces are so homogeneous that there are few distinguishing feature points. In this case, excessively large grid and search areas are likely to cause false matching of feature points. Based on a large amount of experimental analysis, we set the reference window for cross-correlation calculations to 10×10 pixels, which corresponds to a ground distance of 2500 m × 2500 m, and the search area is set to 36×36 pixels, which corresponds to a ground distance of 9000 m × 9000 m.

The cross-correlation calculation is performed after grid segmentation. Available algorithms include Orientation correlation (OC) (Haug et al., 2010), NCC (Kääb et al., 2005), CCF (Heid and Kääb, 2012), and CCC (Huang and Li, 2011). In the present study, we expect to identify the general feature and spatiotemporal variation patterns of Antarctic Peninsula glacier surface movement through large-scale, long-duration velocity estimation. Thus, there is no need for high-accuracy estimation of the velocity of thin ice streams within the glaciers. Furthermore, to reduce the amount of calculation, we chose the simple CCC algorithm that provides moderate accuracy and involves less data processing (Wu et al., 1997; Evans, 2000):

$$\mathrm{CCC}(u,v) = \frac{\sum_{y=1}^{M}\sum_{x=1}^{N}[f(x,y)-\bar{f}]}{\left\{\sum_{y=1}^{M}\sum_{x=1}^{N}[f(x,y)-\bar{f}]^2\right\}^{1/2}} \cdot \frac{[g(x+u,y+v)-\bar{g}(u,v)]^2}{\left\{\sum_{y=1}^{M}\sum_{x=1}^{N}[g(x+u,y+v)-\bar{g}(u,v)]^2\right\}^{1/2}} \quad (1)$$

TCD
8, 5875–5910, 2014

where $f(x,y)$ is the pixel value of point P in the reference window of the reference image; $g(x,y)$ is the pixel value of point P′ in the corresponding search window of the search image (Fig. 4); u,v are the distances of window movements in the search image in the x axis and y axis directions, respectively; $\overline{f},\overline{g}(u,v)$ is the average pixel value of matching windows in the reference image and search image, respectively; N,M is the scope of the search area; and $[f(x,y)-\overline{f}]$ and $[g(x+u,y+v)-\overline{g}(u,v)]$ represent the difference between the DN value of each pixel and the average of all pixels within a window, respectively. Thus, when a difference in the overall DN value of two images from two sets of MOD02 data in different time phases occurs, e.g. due to varying of sun elevation angles, sensor angles or system error in atmospheric conditions, the CCC algorithm will automatically eliminate the error influence through differentiation between the individual pixel value and the average value. However, in this method, the definition of a feature point is too absolute, likely causing false matching of feature points (Huang and Li, 2009). Moreover, the Antarctic Peninsula has homogenous glacier surfaces with relatively smooth pixel values. Therefore, atmospheric and terrain corrections will inevitably screen out certain feature points, such as the texture in ice streams and the ice mounds. Hence, we omit the atmospheric and terrain correction steps in the data processing.

In the CCC algorithm, the results of each window calculation are recorded using the north–south and east–west displacement distances and the signal-to-noise ratio (hereafter referred to as SNR), and the results are then saved in a raster format. The pixel resolution of this raster file is the step size of the window movement (each step is a pixel, corresponding to a ground distance of 250 m). The SNR directly records the credibility of this feature tracking calculation (Xu et al., 2011): SNR = 1 indicates perfect correlation in the feature point matching, and SNR = 0 indicates a perfect absence of correlation in the feature point matching. Thus, an SNR value close to 1 indicates high credibility of the calculation results. We remove the results with SNR < 0.7 to ensure the reliability of the correlation calculations.

TCD
8, 5875–5910, 2014

4.2 Surface velocity calculation

Because the time interval of each data set is not a complete year, displacement distance obtained through the above process needs to be converted to an average annual velocity. Using 365 days per year,

$$V_{yr} = \frac{U}{T_d} \times 365 \tag{2}$$

where V_{yr} is the average annual velocity, T_d is the number of days during time interval; and U is the displacement distance.

4.3 Three-dimensional (3-D) terrain correction

The glacier displacement obtained using the CCC algorithm is the projected displacement on the orthophoto. Further, the real displacement is obtained through 3-D terrain correction with ASTER GDEM (Fig. 5).

$$V_{3\text{-}D} = V_{2\text{-}D} / \cos\theta \tag{3}$$

where $V_{2\text{-}D}$ is the in-plane velocity of point P, $V_{3\text{-}D}$ is the 3-D velocity of point P, θ is the slope angle of point P along the movement direction calculated from the DEM (Ke et al., 2013).

4.4 The displacement orientation conversion

The east–west and north–south displacements are obtained using the cross-correlation method, and the direction of glacier movement is calculated using Eq. (4):

$$\theta = 90° \left(2 \left(1 + \frac{|u_{E-W}|}{\pi u_{E-W}} \sin^{-1} \frac{v_{N-S}}{\sqrt{u_{E-W}^2 + v_{N-S}^2}} \right) - \frac{|v_{N-S}|}{v_{N-S}} \left(\frac{|u_{E-W}|}{u_{E-W}} + 1 \right) \right) \tag{4}$$

TCD
8, 5875–5910, 2014

where u_{E-W} is the east–west displacement, with west to east defined as positive, and east to west as negative; and v_{N-S} is the north–south displacement, with south to north defined as positive, and north to south as negative; θ represents the angle between the geographic east ($\theta = 0^{\circ}$) and the moving direction of the glacier surface flow within 0–360°. The fitting function Eq. (4) is obtained by four piecewise functions as follows using the method of undetermined coefficients:

$$\theta = \frac{180^{\circ}}{\pi}\sin^{-1}\frac{v_{N-S}}{\sqrt{u_{E-W}^2 + v_{N-S}^2}} \quad (0 < \theta \le 90^{\circ}) \tag{5}$$

$$\theta = 90^{\circ} + \frac{180^{\circ}}{\pi}\sin^{-1}\frac{|v_{N-S}|}{\sqrt{u_{E-W}^2 + v_{N-S}^2}} \quad (90^{\circ} < \theta \le 180^{\circ}) \tag{6}$$

$$\theta = 180^{\circ} + \frac{180^{\circ}}{\pi}\sin^{-1}\frac{|v_{N-S}|}{\sqrt{u_{E-W}^2 + v_{N-S}^2}} \quad (180^{\circ} < \theta \le 270^{\circ}) \tag{7}$$

$$\theta = 360^{\circ} + \frac{180^{\circ}}{\pi}\sin^{-1}\frac{v_{N-S}}{\sqrt{u_{E-W}^2 + v_{N-S}^2}} \quad (270^{\circ} < \theta \le 360^{\circ}). \tag{8}$$

5 Results and discussion

5.1 The spatial distribution of surface velocities

The cross-correlation calculations of four sets of images produce Antarctic Peninsula glacier surface velocities over four periods, 2000–2003, 2003–2006, 2006–2009, and 2009–2012 (Fig. 6).

The results show that the glaciers of Graham Land and the Larsen Ice Shelf have significantly different velocity features. The glaciers of Graham Land primarily flow from the peninsula ridge toward the east and west into the Weddell Sea and Bellingshausen

TCD
8, 5875–5910, 2014

Sea, respectively. At the sea outfall, glaciers are confined by local terrain conditions into thin valley glaciers (ice stream) in diverse flow directions, eventually flowing into ice shelves and the sea (Fig. 7). However, the peninsula's rugged terrain significantly blocks the glacier flow, and the small glacier mass results in weak longitudinal stress of ice flows. Consequently, the Graham Land glaciers as a whole have lower velocities, with a local minimum of $< 20\,m\,a^{-1}$ and a maximum of $1500\,m\,a^{-1}$ (average 100–150 $m\,a^{-1}$). The Larsen Ice Shelf has an average velocity of 750–800 $m\,a^{-1}$, with a maximum $> 1500\,m\,a^{-1}$. Compared with the glaciers of Graham Land, the Larsen Ice Shelf flows in almost a single direction, mainly along the northeast direction into the Weddell Sea. A very large ice flux and less bottom friction account for the significantly higher velocities of the ice shelf than the inland glaciers.

Furthermore, 50 sampling points evenly distributed across Graham Land and the Larsen Ice Shelf have been chosen for more intuitive analysis of the Antarctic Peninsula ice velocity features (Fig. 8). Average velocities at the sampling points are obtained from four sets of inverse velocity contour maps (Fig. 9). As observed, the individual sampling points of Graham Land have discretely distributed velocities, despite their generally low level as a whole. The discrete distribution pattern is possibly the result of the rugged terrain of the narrow Antarctic Peninsula and the differences in ice flux as well as subglacial supporting conditions of the ice shelves. Even the same ice stream at different altitudes has substantial differences in flow velocity. The velocities of ice streams in the upstream regions are relatively low, and the velocities sharply increase when the ice sheet mass converges with numerous tiny ice flows moving toward the sea. For example, the velocities at the upstream reaches of the Crane Glacier are $< 150\,m\,a^{-1}$, while those near the outfall approach $1500\,m\,a^{-1}$ (Scambos et al., 2004). As for the Larsen Ice Shelf, the sampling points not only have relatively high velocities as a whole but also exhibit more convergent distribution of individual velocities.

TCD
8, 5875–5910, 2014

5.2 Temporal variations in surface velocities

In terms of temporal distribution (Fig. 10), the Graham Land glaciers exhibit complex ice velocity changes at different sampling points. Over the period between 2000 and 2012, the majority of the sampling points showed accelerations, with an average speed increase of 13.5 %. This acceleration was slightly higher than that reported by Pritchard et al. (2007), who estimated an average speed increase of 12 % for more than 300 glaciers during 1992–2005. The acceleration was mainly because rapid disintegration of the Larsen Ice Shelf in large areas led to rapid flow of the upstream-supplied glaciers. In particular, the large-scale disintegration of the Larsen B Ice Shelf at the end of the last century caused a speed increase of 35 % in the upstream Crane Glacier over the period 2000–2012. In addition, surface melting and massive bottom melting near the grounding line contributed to the acceleration of the ice sheet flows (Rignot et al., 2008). Generally speaking, glacial acceleration is a common phenomenon in the Antarctic. For example, the Thwaites Glacier Tongue accelerated from 2680 m a^{-1} over the period 1972–1984 to 2950 m a^{-1} in 2006 (Rosanova et al., 1998), whereas the Haynes and Smith glaciers accelerated by 27 and 75 %, respectively, from 1996 to 2006. In particular, the Smith Glacier experienced a speed increase by 8 % over the one-year period 2006–2007 (Rignot, 2008). In the northern part of the peninsula, there were five sampling points associated with a decrease in the average velocity. The slowdown was possibly related to strong, rapid thinning of the ice sheet mass in local areas. Mass reduction can cause weakening of the longitudinal stress and thus lead to unexpected slowdown. This slowdown feature is also present in the Siple Coast C ice streams and the Whillans ice streams (Bindschadler et al., 1996).

The sampling points on the Larsen Ice Shelf clearly accelerated over time, with an average velocity increase of 13 % from 2000 to 2006 and 15 % from 2006 to 2012. These speed increases were greater than those estimated for the period 1988–1994 and 1994–1997, i.e. 13.2 % (Kvarcaet et al., 1999). Our results coincided with previous estimates of the change pattern by Vieli et al. (2006), who reported that the Larsen B

TCD
8, 5875–5910, 2014

shelf accelerated by 150 m a^{-1} from 1995–1999. It is due mainly to rapid disintegration of the ice shelf itself that led to the faster flowing ice streams (Stephenson and Bindschadler, 1988; Rignot et al., 2008).

5.3 Error analysis

Due to restrictions of natural conditions, less in situ measurement data are available for the Antarctic Peninsula. The results obtained using remote sensing methods are mainly focused on single glaciers (ice streams). In the present study, the average velocity, i.e. 850–1350 m a^{-1} of the downstream Crane Glacier in 2002–2003 is estimated based on MODIS data (Fig. 11). This result is consistent with the estimate of downstream Crane Glacier in 2001–2002 based on TM images, i.e. 950–1500 m a^{-1} (Scambos et al., 2004). As for individual ice streams, velocity estimation based on MODIS data has slightly lower accuracy. However, the average velocity of the Larsen B Ice Shelf during 2000–2012 is estimated to be 350–450 m a^{-1} (Fig. 12), which coincides with the results previously estimated using high-resolution image data, i.e. an average velocity of 370 m a^{-1} during 2002–2006 and an acceleration of 400 m a^{-1} from 2006 to 2009 (Haug et al., 2010; Scambos et al., 2004).

The velocity-estimation method of a single glacier used in this study has relatively low accuracy relative to other methods such as high-resolution optical image feature tracking (Lucchitta and Rosanova, 1997; Frezzotti et al., 1998), InSAR (Fricker et al., 2009), and GPS. However, this method can still achieve satisfactory results in open areas of ice shelf regions that have significant flowing texture. Nonetheless, there are a few constraints for this method.

With regard to image quality, the Antarctic Peninsula experiences frequent mass exchange with the ocean, leading to cloudy, snowy weather almost year-round. It is therefore very difficult to obtain optical images of high quality for cross-correlation calculations. Here, we chose cross-correlation images with $< 10\,\%$ cloud cover from massive quantities of data from 2000, 2003, 2006, 2009, and 2012. However, the cloud cover

TCD
8, 5875–5910, 2014

conditions in local areas are not ideal, affecting the accuracy of the regional feature tracking to some extent.

From the perspective of feature point defects, the correlation calculation of glacier movement mainly involves moraine deposits, ice cracks, crevasses, and ice mounds. As indicated above, the surface of the Antarctic ice sheet is very uniform with much fewer moraines than valley glaciers. Additionally, a large amount of snow accumulates on the glacier surface, which can cover surface feature points (Esra et al., 2009). Compared with valley glaciers, ice shelf regions lack evident textural features due to the flat terrain and very large ice stream mass. Moreover, false matching of feature points may occur in ice shelves due to vertical variations caused by freeze-melt and seawater tides (Yu et al., 2010).

Another possible source of error may be related to the micro-terrain. The terrain of the Antarctic Peninsula is rugged, forming many small ice streams, such as the Hektoria and Green glaciers. Their widths only occupy a few pixels of the MODIS images, whereas the grid segmentation of the cross-correlation calculation requires a certain number of pixels to ensure accuracy. Hence, feature tracking based on medium-resolution optical images may be ineffective for velocity estimation of very small ice streams of the Antarctic ice sheet (Scherler et al., 2008).

The above limitations can impact the accuracy of the glacier surface velocity estimation for the Antarctic Peninsula, resulting in abnormal velocities at a few sampling points (Fig. 9). However, CCC algorithm using medium-resolution optical images is a very useful tool in studying the spatiotemporal variations in large-scale glacier movement in the Antarctic ice sheet area.

6 Conclusions

This study estimates glacier velocities in the Antarctic Peninsula using COSI-Corr based on MODIS L1B data from years 2000, 2003, 2006, 2009, and 2012. The results show that the Graham Land glaciers and the Larsen Ice Shelf have distinctive velocity

TCD
8, 5875–5910, 2014

features. The glaciers of Graham Land as a whole have low velocities, with an average of 100–150 m a^{-1}. Due to the rugged nature of the underlying terrain and different quantities of glacier mass, there are tremendous differences in ice velocities among the Graham Land glaciers, as reflected by a maximum of approximately 1500 m a^{-1} and a minimum of < 20 m a^{-1}. As for the Larsen Ice Shelf, the overall velocity is relatively high due to the very large ice flux and lower bottom friction near the grounding line. The Larsen Ice Shelf has an average velocity of 750–800 m a^{-1} with a maximum of > 1500 m a^{-1}, making it one of the fastest-moving regions in the Antarctic ice sheet. The Graham Land glacier velocities experienced complex changes over time. Due to downstream glacier mass loss, the average velocity increased by 13.5 % from 2000 to 2012 in the southern part of the Peninsula. Certain glaciers even accelerated by 30 %, whereas local areas in the northern part of the peninsula experienced velocity decreases. The latter phenomenon could be related to the reduction of longitudinal stress caused by the rapid thinning of glaciers. In recent years, the Larsen Ice Shelf has rapidly disintegrated on a large scale. Together, glacier surface melt and strong bottom melting (Rignot et al., 2008) near the grounding line have contributed to the acceleration of ice shelves and upstream-supplied glaciers. The average velocity of the Larsen Ice Shelf increased by 13 % from 2000 to 2006 and by 15 % from 2006 to 2012.

MODIS data can be used to continuously monitor the glacier surface velocities of the Antarctic Peninsula over large spatial scales and for long time series. MODIS L1B has clear advantages in large-scale macroscopic research of spatiotemporal variations in the Antarctic ice sheet movement. Satisfactory results are estimated especially for the Larsen Ice Shelf. However, due to issues related to clouds, feature point defects, micro-terrain, and the simplicity of the CCC algorithm, certain level of errors occur in the velocity estimates of the Graham Land glaciers.

Acknowledgements. This work was supported by Program for National Nature Science Foundation (No. 41371391), Program for Chinese National Antarctic and Arctic Research Expedition (CHINARE2014-02-02), Program for the Specialized Research Fund for the Doctoral Program of Higher Education of China (No. 20120091110017) and A Project Funded by the

TCD
8, 5875–5910, 2014

PriorityAcademicProgram Development of Jiangsu Higher Education Institutions (PAPD). And this work was partially supported by Collaborative Innovation Center of Novel Software Technology and Industrialization.

References

Ahn, Y. and Howat, I. M.: Efficient automated glacier surface velocity measurement from repeat images using multi-image/multichip and null exclusion feature tracking, IEEE T. Geosci. Remote, 49, 2838–2846, doi:10.1109/TGRS.2011.2114891, 2010.

Bamber, J. L., Riva, R. E. M., Vermeersen, B. L. A., and LeBrocq, A. M.: Reassessment of the potential sea-level rise from a collapse of the West Antarctic Ice Sheet, Science, 324, 901–903, doi:10.1126/science.1169335, 2009.

Berthier, E., Raup, B., and Scambos, T. A.: New velocity map and mass-balance estimate of Mertz Glacier, East Antarctica, derived from Landsat sequential imagery, J. Glaciol., 49, 503–511, doi:10.3189/172756503781830377, 2003.

Brown, L. G.: A survey of image registration techniques, Comput. Surv., 24, 325–376, doi:10.1145/146370.146374, 1992.

Bindschadler, R. A., Vornberger, P., Blankenship, D., Scambos, T. A., and Jacobel, R.: Surface velocity and mass balance of Ice Streams D and E, West Antarctica, J. Glaciol., 42, 461–475, 1996.

Bindschadler, R. A., Scambos, T. A., Rott, H., Skvarca, P., and Vornberger, P.: Ice dolines on Larsen Ice Shelf, Antarctica, Ann. Glaciol., 34, 283–290, doi:10.3189/172756402781817996, 2002.

Cheng, X., Li, X., Shao, Y., and Li, Z.: DINSAR measurement of glacier motion in Antarctic Grove Mountain, Chinese Sci. Bull., 52, 358–366, doi:10.1007/s11434-007-0054-y, 2007.

Djamel, A. and Hammadi, A.: External Validation of the ASTER GDEM2, GMTED2010 and CGIAR-CSI-SRTM v4.1 free access Digital Elevation Models (DEMs) in Tunisia and Algeria, Remote Sens., 6, 4600–4620, doi:10.3390/rs6054600, 2014.

Dong, C. E., Zhou, C. X., and Liao, M. S.: Application of SAR interferometry in Grove Mountains, East Antarctica, Ann. Glaciol., 23, 514–521, doi:10.1117/12.514161, 2004.

Dorrer, E., Hofmann, W., and Seufert, W.: Geodetic results of the Ross Ice Shelf survey expeditions, 1962–1963 and 1965–1966, J. Glaciol., 52, 67–90, 1969.

TCD
8, 5875–5910, 2014

Dyurgerov, B. and Meier, M. F.: Twentieth century climate change: evidence from small glaciers, P. Natl. Acad. Sci. USA, 97, 1406–1411, doi:10.1073/pnas.97.4.1406, 2000.
Erten, E., Chesnokova, O., Hajnsek, I., and Reigber, A.: Glacier surface velocity measure based on polarimetric tracking, Ann. Glaciol., 12, 3126–3129, doi:10.1109/IGARSS.2012.6350763, 2012.
Esra, E., Andreas, P., Olaf, H., and Pau, P.: Glacier velocity monitoring by maximum likelihood texture tracking, IEEE T. Geosci. Remote, 47, 394–405, doi:10.1109/TGRS.2008.2009932, 2009.
Evans, A. N.: Glacier surface motion computation from digital image sequences, IEEE T. Geosci. Remote, 38, 1064–1072, doi:10.1109/36.841985, 2000.
Ferrigno, J. G., Mullins, J. L., Stapleton, J. A., Bindschadler, R. A., Scambos, T. A., Bellisime, L. B., Bowell, J. A., and Acosta, A. V.: Landsat TM image maps of the Shirase and Siple Coast Ice Streams, West Antarctica, Ann. Glaciol., 20, 407–412, doi:10.3189/172756494794587087, 1994.
Ferrigno, J. G., Williams, R. S., Rosanova, C. E., Lucchitta, B. K., and Swithinbank, C.: Analysis of coastal change in Marie Byrd Land and Ellsworth Land, West Antarctica, using Landsat imagery, Ann. Glaciol., 27, 33–40, 1998.
Frezzotti, M. A., Capra, A., and Vittuari, L.: Comparison between glacier ice velocities inferred from GPS and sequential satellite images, Ann. Glaciol., 27, 54–60, 1998.
Fricker, H. A., Coleman, R., Padman, L., Scambos, T. A., Bohlander, J., and Brunt, K. M.: Mapping the grounding zone of the Amery Ice Shelf, east Antarctica using InSAR, MODIS and ICESat, Antarct. Sci., 21, 515–532, doi:10.1017/S095410200999023X, 2009.
Haug, T., Kääb, A., and Skvarca, P.: Monitoring ice shelf velocities from repeat MODIS and Landsat data – a method study on the Larsen C ice shelf, Antarctic Peninsula, and 10 other ice shelves around Antarctica, The Cryosphere, 4, 161–178, doi:10.5194/tc-4-161-2010, 2010.
Heid, T. and Kääb, A.: Evaluation of existing image matching methods for deriving glacier surface displacements globally from optical satellite imagery, Remote Sens. Environ., 118, 339–355, doi:10.1016/j.rse.2011.11.024, 2012.
Hofmann, W., Dorrer, E., and Nottarp, K.: The Ross Ice Shelf survey (RISS) 1962–1963, in Antarctic snow and ice studies, J. Glaciol., 45, 83–117, 1964.

TCD
8, 5875–5910, 2014

Holger, F. and Frank, P.: On the suitability of the SRTM DEM and ASTER GDEM for the compilation of topographic parameters in glacier inventories, Int. J. Appl. Earth Obs., 18, 480–490, doi:10.1016/j.jag.2011.09.020, 2012.
Huang, L. and Li, Z.: Mountain glacier flow velocities analyzed from satellite optical images, J. Glaciol. Geocryol., 31, 935–940, 2009.
Huang, L. and Li, Z.: Comparison of SAR and optical data in deriving glacier velocity with feature tracking, Int. J. Remote Sens., 33, 2681–1698, doi:10.1080/01431161003720395, 2011.
Kääb, A., Lefauconnier, B., and Melvold, K.: Flow field of Kronebreen, Svalbard, using repeated Landsat 7 and ASTER data, Ann. Glaciol., 42, 7–13, doi:10.3189/172756405781812916, 2005.
Kang, X. W. and Feng, Z. K.: An introduction to ASTER GDEM and procedure reading, Appl. Remote Sens., 6, 69–72, 2011.
Ke, C. Q., Kou, C., Ludwig, R., and Qin, X.: Glacier velocity measurements in the eastern Yigong Zangbo basin, Tibet, China, J. Glaciol., 59, 1060–1068, doi:10.3189/2013JoG12J234, 2013.
Khazendar, A., Rignot, E., and Larour, E.: Acceleration and spatial rheology of Larsen C Ice Shelf, Antarctic Peninsula, Geophys. Res. Lett., 38, L09502, doi:10.1029/2011GL046775, 2011.
Kimura, H., Kanamori, T., Wakabayashi, H., and Nishio, F.: Ice sheet motion in inland Antarctica from JERS-1 SAR interferometry, Int. Geosci. Remote Se., 1–7, 3018–3020, doi:10.1109/IGARSS.2004.1370332, 2004.
Liu, H. X., Wang, L., Tang, S. J., and Jezek, K. C.: Robust multi-scale image matching for deriving ice surface velocity field from sequential satellite images, Int. J. Remote Sens., 33, 1799–1822, doi:10.1080/01431161.2011.602128, 2012.
Lucchitta, B. K. and Rosanova, C. E.: Velocities of Pine Island and Thwaites Glaciers, West Antarctica, from ERS-1 SAR images, Ann. Glaciol., 21, 819–824, 1997.
Lucchitta, B. K., Mullins, K. F., Allison, A. L., and Ferrigno, J. G.: Antarctic glacier-tongue velocities from Landsat images-1st result, Ann. Glaciol., 27, 356–366, 1993.
Manson, R., Coleman, R., Morgan, P., and King, M.: Ice velocities of the Lambert Glacier from static GPS observations, Earth Planets Space, 52, 1031–1036, 2000.

TCD
8, 5875–5910, 2014

Meredith, M. P. and King, J. C.: Rapid climate change in the ocean west of the Antarctic Peninsula during the second half of the 20th century, Geophys. Res. Lett., 32, L19604, doi:10.1029/2005GL024042, 2005.
Ni, W. J., Zhang, Z. Y., Sun, G. Q., Guo, Z. F., and He, Y. T.: The penetration depth derived from the synthesis of ALOS/PALSAR InSAR data and ASTER GDEM for the mapping of forest biomass, Remote Sens., 6, 7303–7319, doi:10.3390/rs6087303, 2014.
Osmanoglu, B.: Surface velocity and ice discharge of the ice cap on King George Island, Antarctica, Ann. Glaciol., 54, 111–119, doi:10.3189/2013AoG63A517, 2013.
Pattyn, F. and Derauw, D.: Ice–dynamic conditions of Shirase Glacier, Antarctica, inferred from ERS SAR interferometry, J. Glaciol., 48, 559–565, doi:10.3189/172756502781831115, 2002.
Pritchard, H. D. and Vaughan, D. C.: Widespread acceleration of tide water glaciers on the Antarctic Peninsula, J. Geophys. Res., 112, 1029–1031, doi:10.1029/2006JF000597, 2007.
Rack, W., Rott, H., Siegel, A., and Skvarca, P.: The motion field of northern Larsen Ice Shelf, Antarctic Peninsula, derived from satellite imagery, Ann. Glaciol., 29, 261–266, doi:10.3189/172756499781821120, 1999.
Rosanova, C. E., Lucchitta, B. K., and Ferrigno, J. G.: Velocities of Thwaites Glacier and smaller glaciers along the Marie Byrd Land coast, West Antarctica, Ann. Glaciol., 27, 47–53, 1998.
Rosenau, R., Dietrich, R., and Baessler, M.: Temporal flow variations of major outlet glaciers in Greenland using Landsat data, Int. Geosci. Remote Se., 23, 1557–1560, doi:10.1109/IGARSS.2002.1025771, 2012.
Rignot, E.: Changes in west Antarctic ice stream dynamics observed with ALOS PALSAR data, Geophys. Res. Lett., 35, 63–74, doi:10.1029/2008GL033365, 2008.
Rignot, E., Casassa, G., and Gogineni, S.: Accelerated ice discharge from the Antarctic Peninsula following the collapse of Larsen B ice shelf, Geophys. Res. Lett., 32, 1–4, doi:10.1029/2004GL020697, 2004.
Rignot, E., Bamber, J. L., Van Den Broeke, M. R., Davis, C., Li, Y. H., Van De Berg, W. J., and Van Meijgaard, E.: Recent Antarctic ice mass loss from radar interferometry and regional climate modelling, Nat. Geosci., 1, 106–110, doi:10.1038/ngeo102, 2008.
Rignot, E., Mouginot, J., and Scheuchl, B.: Ice flow of the Antarctic Ice Sheet, Science, 9, 1427–1430, doi:10.1126/science.1208336, 2011.

TCD
8, 5875–5910, 2014

Saraswat, P., Syed, T. H., Famiglietti, J. S., Fielding, E. J., Crippen, R., and Gupta, N.: Recent changes in the snout position and surface velocity of Gangotri glacier observed from space, Int. J. Remote Sens., 34, 8653–8668, doi:10.1080/01431161.2013.845923, 2013.
Scambos, T. A., Dutkiewicz, M. J., Wilson, J. C., and Bindschadler, R. A.: Application of image cross-correlation to the measurement of glacier velocity using satellite image data, Remote Sens. Environ., 42, 177–186, doi:10.1016/0034-4257(92)90101-O, 1992.
Scambos, T. A., Bohlander, J. A., Shuman, C. A., and Skvarca, P.: Glacier acceleration and thinning after ice shelf collapse in the Larsen B embayment, Antarctica, Geophys. Res. Lett., 31, L18402, doi:10.1029/2004GL020670, 2004.
Scherler, D., Leprince, S., and Strecker, M. R.: Glacier-surface velocities in alpine terrain from optical satellite imagery-Accuracy improvement and quality assessment, Remote Sens. Environ., 112, 3806–3819, doi:10.1016/j.rse.2008.05.018, 2008.
Scheuchl, B., Mouginot, J., and Rignot, E.: Ice velocity changes in the Ross and Ronne sectors observed using satellite radar data from 1997 and 2009, The Cryosphere, 6, 1019–1030, doi:10.5194/tc-6-1019-2012, 2012.
Shi, Y. F. and Liu, S. Y.: Chinese glacier response to global warming in the 21st century estimate, Chinese Sci. Bull., 45, 434–438, 2000.
Skvarca, P., Rack, W., and Rott, H.: 34 year satellite time series to monitor characteristics, extent and dynamics of Larsen B Ice Shelf, Antarctic Peninsula, Ann. Glaciol., 29, 255–260, doi:10.3189/172756499781821283, 1999.
Slater, J. A., Heady, B., Kroenung, G., Curtis, W., Haase, J., Hoegemann, D., Shockley, C., and Tracy, K.: Evaluation of the New ASTER Global Digital Elevation Model, National Geospatial-Intelligence Agency, Springfield, VA, USA, 2009.
Stephenson, S. N. and Bindschadler, R. A.: Observed velocity fluctuations on a major Antarctic ice stream, Nature, 334, 695–697, doi:10.1038/334695a0, 1988.
Sunil, P. S.: GPS determination of the velocity and strain–rate fields on Schirmacher Glacier, central Dronning Maud Land, Antarctica, J. Glaciol., 53, 558–564, doi:10.3189/002214307784409199, 2007.
Tiwari, R. K., Gupta, R. P., and Arora, M. K.: Estimation of surface ice velocity of Chhota-Shigri glacier using sub-pixel ASTER image correlation, Curr. Sci. India, 106, 853–859, 2014.
Turner, J., Colwell, S. R., Marshall, G. J., Lachlan-Cope, T. A., Carleton, A. M., Jones, P. D., Lagun, V., Reid, P. A., and Iagovkina, S.: Antarctic climate change during the last 50 years, Int. J. Climatol., 25, 279–294, doi:10.1002/joc.1130, 2005.

TCD
8, 5875–5910, 2014

Urbini, S.: Historical behaviour of Dome C and Talos Dome (East Antarctica) as investigated by snow accumulation and ice velocity measurements, Global Planet. Change, 60, 576–588, doi:10.1016/j.gloplacha.2007.08.002, 2008.

Van, P. N., Michel, R., Binet, R., Avouac, J. P., and Taboury, J.: Measuring earthquakes from optical satellite images, Appl. Optics, 39, 3486–3494, doi:10.1364/AO.39.003486, 2000.

Vieli, A., Payne, A. J., Du, Z. J., and Shepherd, A.: Numerical modelling and data assimilation of the Larsen B ice shelf, Antarctic Peninsula, Philos. T. Roy. Soc. A, 364, 1815–1839, doi:10.1098/rsta.2006.1800, 2006.

Wang, Q. H., E, D. C., and Chen, C. M. Antarctic traverses from Zhongshan Station to Dome-A and the results analysis for the GPS points along the expedition route, Geomat. Inform. Sci. Wuhan Univ., 26, 200–231, 2001.

Wu, Q. X., Mcneil, S. J., and Pairman, D.: Correlation and relaxation labelling: an experimental investigation on fast algorithms, Int. J. Remote Sens., 18, 651–662, doi:10.1080/014311697218980, 1997.

Xu, J. L., Zhang, S. Q., Han, H. D., Liu, S. Y., and Zhang, Y. S.: Change of the surface velocity of Koxkar Baxi Glacier interpreted from remote sensing data, Tianshan Mountains, J. Glaciol. Geocryol., 33, 268–275, 2011.

Yu, J., Liu, H. X., Jezek, K. C., Warner, R. C., and Wen, J.: Analysis of velocity field, mass balance, and basal melt of the Lambert Glacier–Amery Ice Shelf system by incorporating Radarsat SAR interferometry and ICESat laser altimetry measurements, J. Geophys Res.-Sol. Ea., 115, 11–12, doi:10.1029/2010JB007456, 2010.

Zhou, C. X., Zhou, Y., Deng, F. H., Ai, S. T., Wang, Z. M., and E, D. C.: Seasonal and interannual ice velocity changes of Polar Record Glacier, East Antarctica, Ann. Glaciol., 55, 45–51, doi:10.3189/2014AoG66A185, 2014.

TCD
8, 5875–5910, 2014

Table 1. The selected MODIS L1B images and their parameters.

Date (UTC)	MOD02 (band1 L1B)	MOD03 (Geocoding data)
24 Sep 2000 (11:55)	MOD02QKM.A2000267.1155.005.2010045210702	MOD03.A2000267.1155.005.2010045203838
2 Feb 2003 (11:55)	MOD02QKM.A2003033.1155.005.2010142140853	MOD03.A2003033.1155.005.2010141153231
10 Nov 2006 (12:35)	MOD02QKM.A2006314.1235.005.2010185060650	MOD03.A2006314.1235.005.2010184180221
8 Apr 2009 (14:15)	MOD02QKM.A2009098.1415.005.2010240015041	MOD03.A2009098.1415.005.2010239035045
17 Nov 2012 (12:25)	MOD02QKM.A2012365.1225.005.2012365193752	MOD03.A2012365.1225.005.2012365192846

TCD
8, 5875–5910, 2014

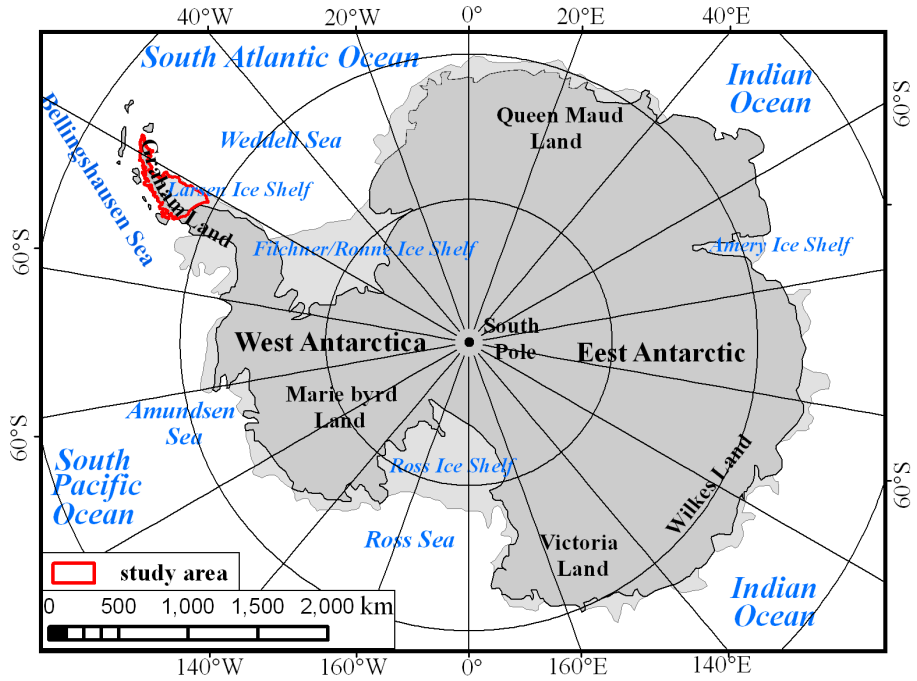

Figure 1. Location of the study area.

TCD
8, 5875–5910, 2014

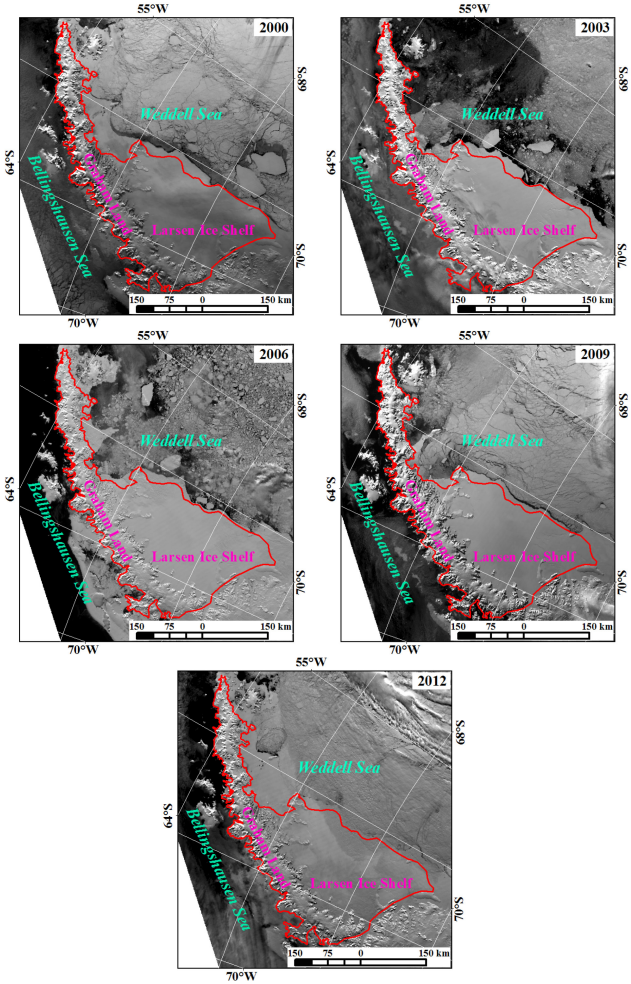

Figure 2. The melt line of the Antarctic Peninsula in different years.

TCD
8, 5875–5910, 2014

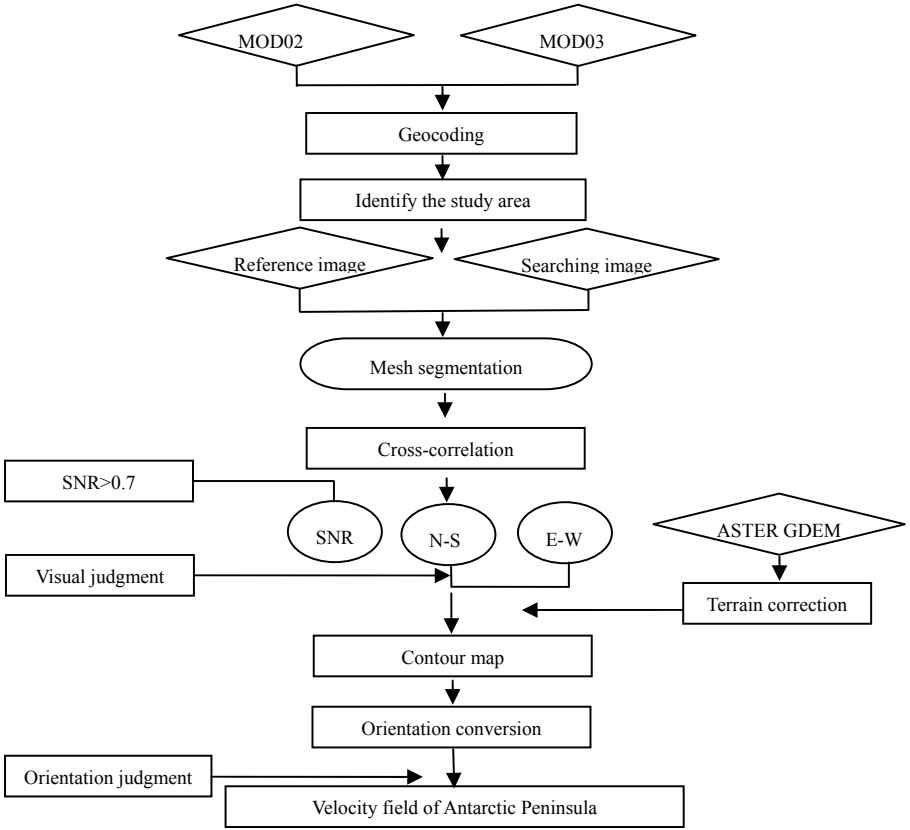

Figure 3. Processing flowchart for deriving glacier surface flow velocities.

TCD
8, 5875–5910, 2014

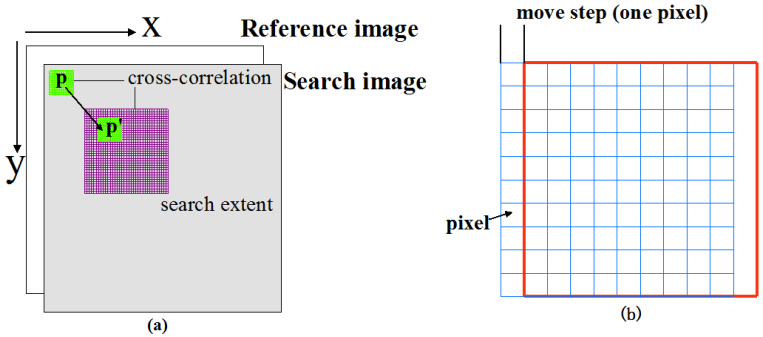

Figure 4. Sketch map of feature tracking.

TCD
8, 5875–5910, 2014

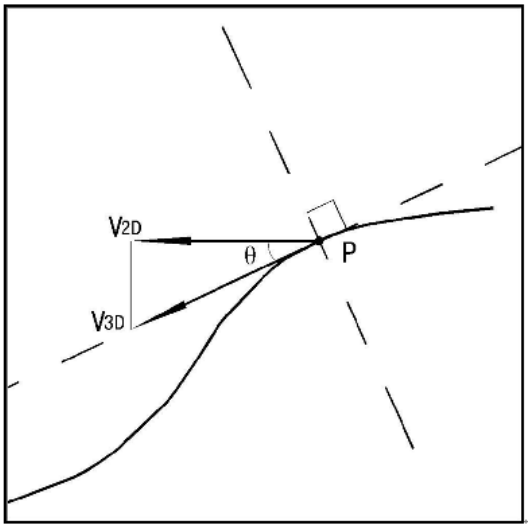

Figure 5. Horizontal velocity and actual velocity of the glacier surface.

TCD
8, 5875–5910, 2014

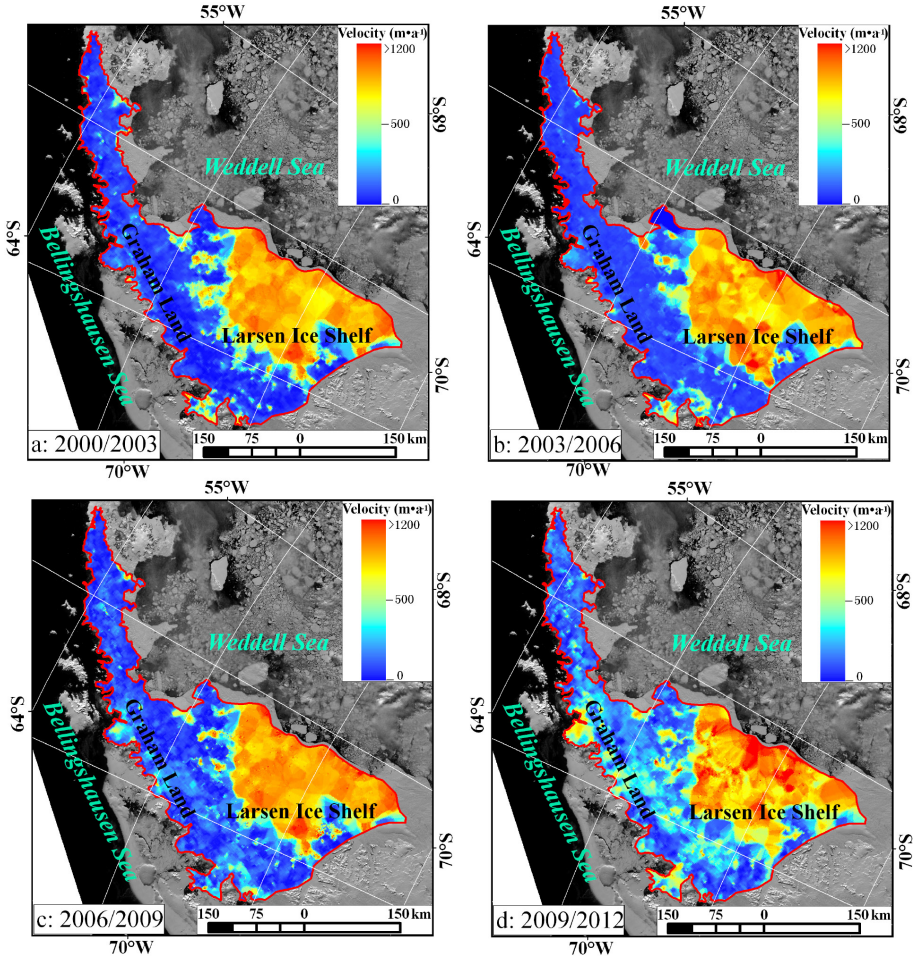

Figure 6. The glacier surface velocity of Antarctic Peninsula.

TCD
8, 5875–5910, 2014

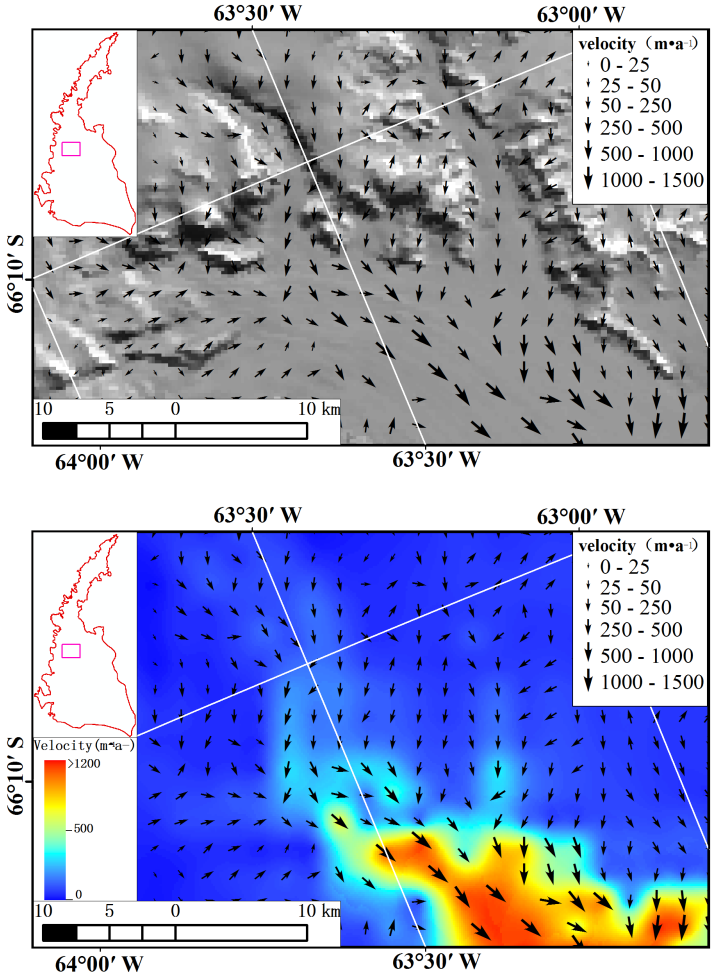

Figure 7. Velocity field of the Antarctic Peninsula (2000/2003).

TCD
8, 5875–5910, 2014

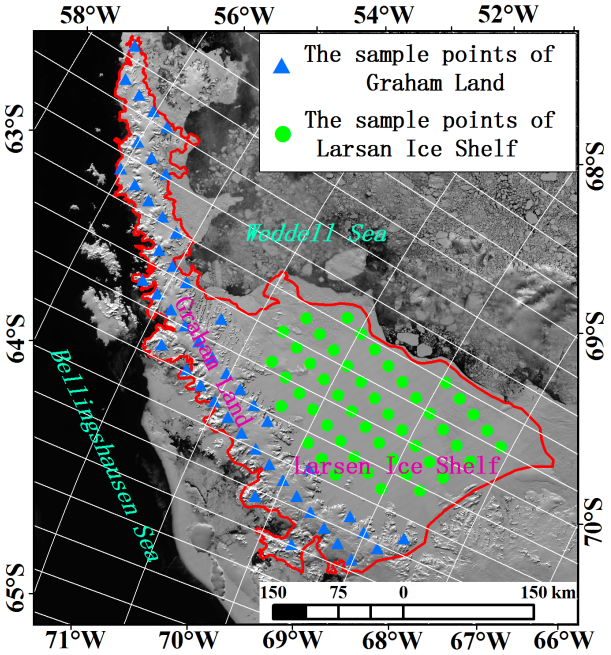

Figure 8. Sketch map of the 50 sample points.

TCD
8, 5875–5910, 2014

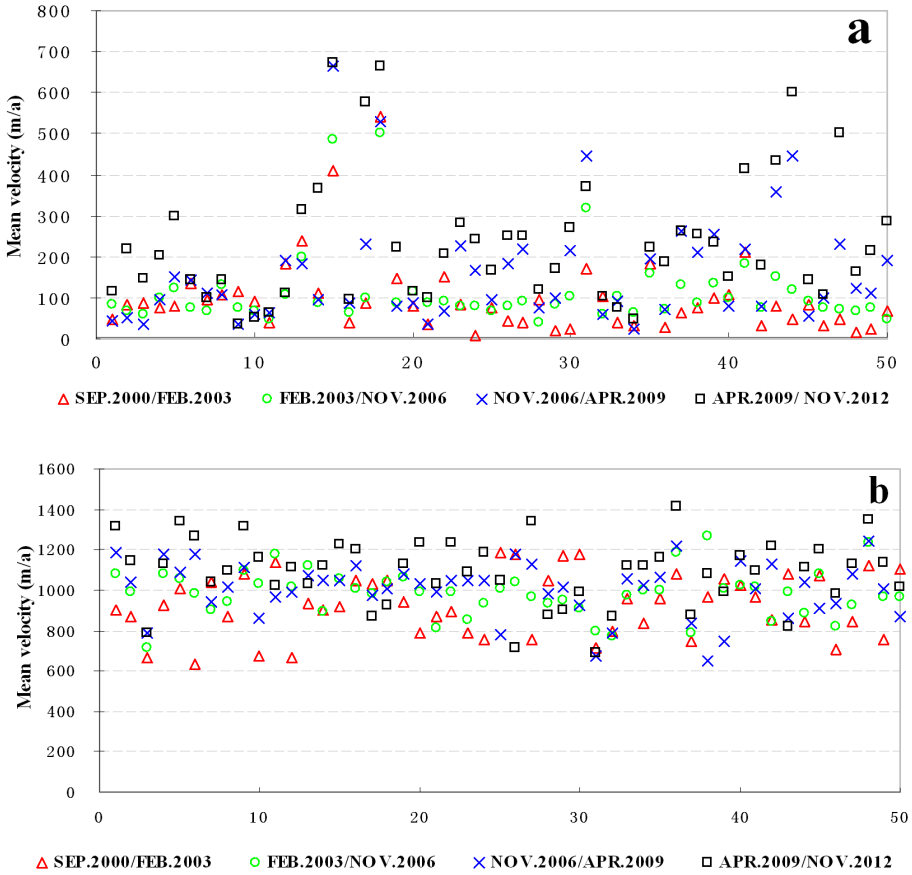

Figure 9. Average annual velocity of the 50 sample points. **(a)** Graham Land, **(b)** Larsen Ice Shelf.

TCD
8, 5875–5910, 2014

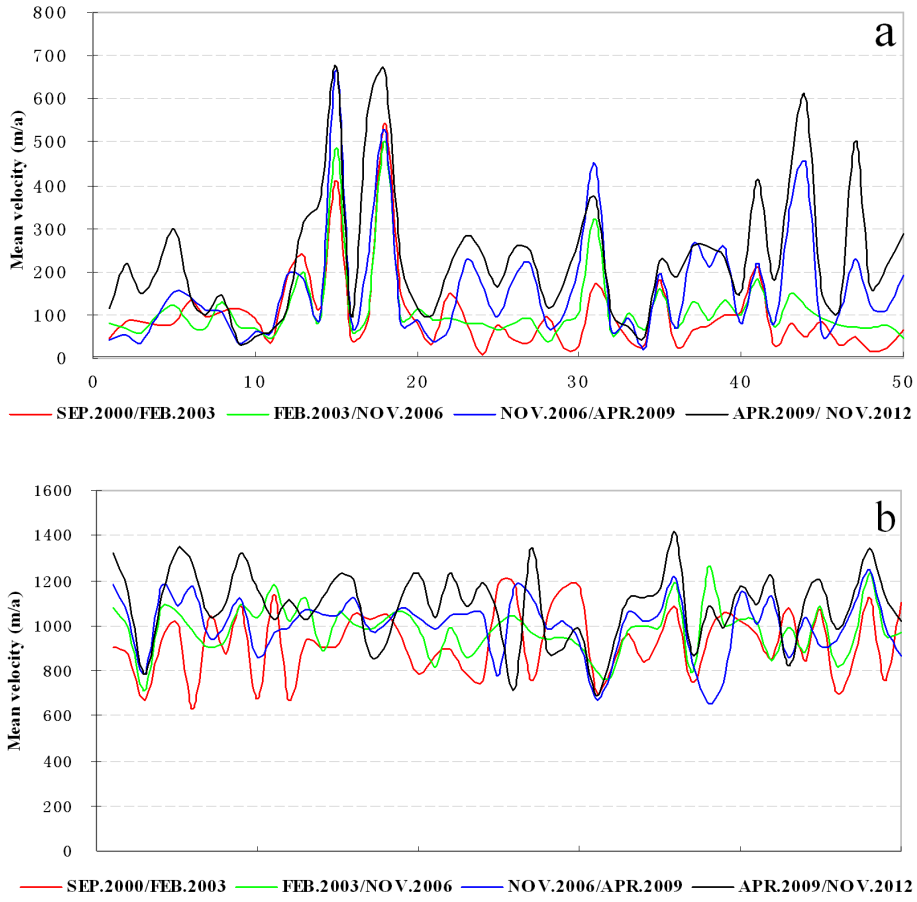

Figure 10. The changing average annual velocities, **(a)** Graham Land, **(b)** Larsen Ice Shelf.

TCD
8, 5875–5910, 2014

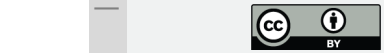

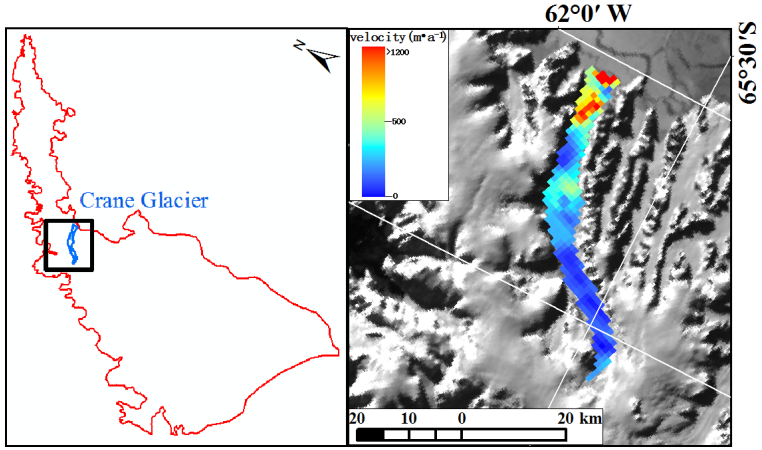

Figure 11. Location of the Crane Glacier and average annual velocity of the Crane Glacier from 2000 to 2003.

TCD
8, 5875–5910, 2014

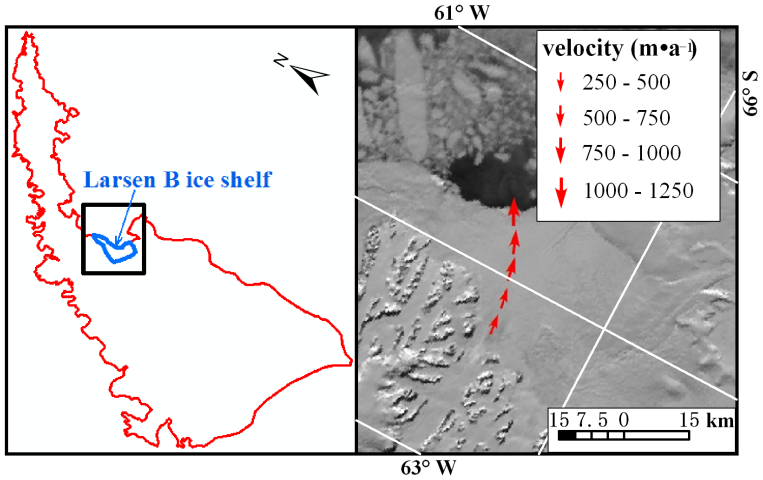

Figure 12. Location of the Larsen B ice shelf and Average annual velocity of the Larsen B ice shelf from 2000 to 2012.

TCD
8, 5875–5910, 2014